Journal of Non-Newtonian Fluid Mechanics 342 (2025) 105438

Contents lists available at ScienceDirect

Journal of Non-Newtonian Fluid Mechanics

journal homepage: www.elsevier.com/locate/jnnfm

Full length article

An insight into parameter identifiability issues in the Carreau–Yasuda model: A more consistent rheological formulation for shear-thinning non-Newtonian inelastic fluids

Gianluca Santesarti [a,b,*], Michele Marino [a], Francesco Viola [c,d], Roberto Verzicco [c,e,f], Giuseppe Vairo [a,g]

[a] University of Rome Tor Vergata, Department of Civil Engineering and Computer Science Engineering, 00133 Rome, Italy
[b] Sapienza University of Rome, Department of Mechanical and Aerospace Engineering, 00184 Rome, Italy
[c] Gran Sasso Science Institute, L'Aquila, 67100, Italy
[d] INFNLaboratori Nazionali del Gran Sasso, Assergi (AQ), 67100, Italy
[e] University of Rome Tor Vergata, Department of Industrial Engineering, 00133 Rome, Italy
[f] Physics of Fluids Group, Max Planck Center for Complex Fluid Dynamics, MESA+ Institute and J. M. Burgers Centre for Fluid Dynamics, University of Twente, P.O. Box 217, 7500AE Enschede, Netherlands
[g] Universidade de Brasília, Department of Mechanical Engineering, 70910-900 Brasília, DF, Brazil

ARTICLE INFO

Keywords:
Non-Newtonian inelastic fluids
Shear-thinning fluids
Rheological modelling
Parameter identifiability properties
Carreau–Yasuda model

ABSTRACT

The Carreau–Yasuda rheological model is widely employed in both research and industrial applications to describe the shear-thinning behaviour of non-Newtonian inelastic fluids. However, the model parameter traditionally employed to characterize the shear thinning response exhibits only a weak correlation with the actual shear thinning rate observed in experimental data. This limitation leads to intrinsic identifiability issues, which may result in misleading physical interpretations of the model parameters and unreliable flow predictions. Aiming to contribute to overcoming these issues, this paper introduces a novel heuristic rheological formulation for shear-thinning non-Newtonian inelastic fluids, as an alternative to the Carreau–Yasuda model. Analytical results and exemplary numerical case studies demonstrate that the proposed formulation is based on physically meaningful model parameters, whose identifiability is not compromised by the key limitations of the Carreau–Yasuda model. The new approach allows for effective parameter estimation through a straightforward direct identification strategy, eliminating the need for inverse identification procedures based on nonlinear regression techniques. Moreover, the proposed formulation naturally enables the identication of two Carreau numbers based on the two characteristic shear rates of the fluid.

1. Introduction

Fluids used in a wide range of advanced applications exhibit a complex non-Newtonian and nonlinear rheological behaviour, characterized by a significant dependence of viscosity on shear rate and/or shear rate history. Typical examples can be found in biomedical engineering [1–3], tribology and industrial processes for the production of lubricants and paints [4], plastic polymer manufacturing [5], food engineering [6]. Among the different types of these complex fluids, in the following reference is made to the class of generalized Newtonian fluids (GNFs), also known as viscous inelastic fluids, that exhibit shear-thinning effects, as for the blood [7,8]. In this case, the actual shear stress depends on the shear rate at the current time and not upon the history of the deformation rate [9], and it can be described via a generalized form of the constitutive equation of Newtonian fluids [5], in which the effective (or apparent) viscosity is a non-linear decreasing function of the shear rate. Specifically, such a nonlinear viscosity response generally exhibits small decreasing rates (thereby corresponding to a quasi-Newtonian behaviour) for both low and high shear rate levels, with a significant nonlinear transition at intermediate shear rates [4,5].

Several empirical models can be found in the specialized literature to describe the rheological behaviour of GNFs with a shear-thinning response. The power-law (or Ostwald–de Waele) model [10,11], defined by two model parameters, expresses the dependence of shear

* Corresponding author.
E-mail addresses: santesarti@ing.uniroma2.it (G. Santesarti), m.marino@ing.uniroma2.it (M. Marino), francesco.viola@gssi.it (F. Viola), verzicco@uniroma2.it (R. Verzicco), vairo@ing.uniroma2.it (G. Vairo).

https://doi.org/10.1016/j.jnnfm.2025.105438
Received 3 March 2025; Received in revised form 10 May 2025; Accepted 13 May 2025
Available online 30 May 2025

stress on shear rate via a power law. It generally provides a suitable description of the nonlinear viscosity behaviour in flow regimes characterized by intermediate shear rates. The Carreau model based on molecular theoretical considerations [12] and the Ellis model [5,13], are both formulated by introducing three model parameters. They capture the transition from the quasi-Newtonian regime at low shear rates to the highly nonlinear trend as the shear rate increases. The Cross model [14], defined by four model parameters, allows to capture the transitions between the quasi-Newtonian regime and the non-Newtonian one at both low and high shear rates. The Carreau–Yasuda model [5,15], also known as the Bird–Cross–Carreau–Yasuda (BCCY) model [16], aims to provide a comprehensive description of the shear-thinning behaviour by combining both the Cross and Carreau models and introducing the additional Yasuda parameter [15].

Specifically addressing the BCCY model, it is generally considered to be effective and highly versatile in describing the shear-thinning trend of complex fluids. It has been widely adopted in many advanced inherent applications, for instance, hemodynamics [8], plastic manufacturing [17], lubricant production [18], and food processing [19]. However, as highlighted by Gallagher et al. [16] in the context of the dynamics of the hematologic fluid, the BCCY model exhibits intrinsic limitations related to the identifiability of the parameters. The identifiability is defined as the capability to find a unique set of model parameters from experimental data gathered from a real system [20–23]. This property is a critical aspect of the modelling process when model parameters are related to physical features of the analysed system (i.e., the fluid rheological properties) [20,22,23]. Specifically, Gallagher et al. [16] found that fitting experimental data using standard nonlinear regression procedures can yield multiple sets of model parameters that provide nearly identical fits of rheological data. This is due to the presence of large, flat regions in the cost surface around the optimal state. Despite producing almost indistinguishable rheological fits, these parameter variations can lead to significantly different and unreliable flow predictions, making it impossible to draw meaningful conclusions about the physical properties of the fluid. Furthermore, when the BCCY model is used to calibrate piecewise approximations — based on the assumption of a sharp viscosity transition between ideal Newtonian regions (at low and high shear rates) and a power-law behaviour at intermediate shear rates, which could be used to derive analytical solutions [24] — additional inconsistencies in parameter interpretation can arise, as it will be analysed in the following. These inconsistencies compromise the physical meaning and applicability of the estimated parameters, further limiting the robustness and reliability of the BCCY model in such scenarios.

In order to contribute to overcoming these identifiability issues, this paper proposes a novel heuristic rheological description for shear-thinning inelastic fluids. Comparisons based on analytical closed-form assessments and numerical optimization procedures — considering both direct and inverse identification strategies — highlight the accuracy and reliability of the proposed rheological model. In particular, the results emphasize the clear physical significance of the model parameters and specifically of the shear-thinning index that predominantly influence the nonlinear response at intermediate shear rate levels. Moreover, they demonstrate that the proposed formulation is highly accurate and efficient even with a simple direct parameter estimation from experimental data, without requiring nonlinear regression procedures. Furthermore, unlike classical approaches that typically refer to a single Carreau number [25,26], the proposed formulation naturally allows for the identification of two distinct Carreau numbers, each associated with one of the fluid's characteristic shear rates.

The paper is organized as follows. Section 2 presents a critical analysis of the BCCY formulation. In Section 3, the novel shear-based rheological model is introduced, with analytical developments (complemented by Appendix) providing theoretical insights into the improved physical interpretability of its parameters. Section 4 discusses identifiability performance and numerical comparisons between the proposed description and the BCCY model, presenting results of direct and inverse parameter estimation procedures based on available experimental data, and analysing their impact on a representative flow case study. Finally, concluding remarks are provided in Section 5.

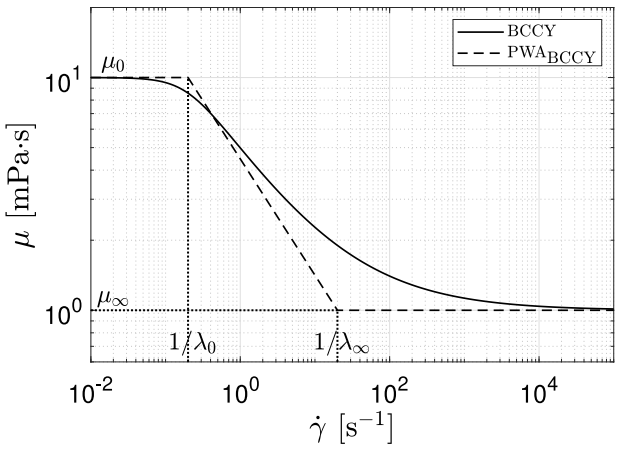

Fig. 1. Example case of the Bird–Cross–Carreau–Yasuda (BCCY) shear-thinning description in comparison with a power-law-based piecewise approximation defined in terms of the BCCY model parameters (PWA$_{\text{BCCY}}$), i.e. by considering $N = n$, $\lambda_0 = \lambda$, $\lambda_\infty = \lambda(\mu_\infty/\mu_0)^{1/(1-n)}$, $K = \mu_0\lambda^{n-1}$. Values of model parameters: $\mu_0 = 10\,\text{mPa s}$, $\mu_\infty = 1\,\text{mPa s}$, $\lambda = 5\,\text{s}$, $n = 0.5$, $a = 2.0$.

2. An insight into the Carreau–Yasuda model

For incompressible GNFs, the constitutive relationship between the deviatoric stress tensor $\boldsymbol{\tau}$ and the strain-rate tensor $\boldsymbol{E}$ results in [5]

$$\boldsymbol{\tau}(\dot{\gamma}) = 2\mu(\dot{\gamma})\,\boldsymbol{E} = \mu(\dot{\gamma})\,\left(\nabla\boldsymbol{v} + \nabla^T\boldsymbol{v}\right), \tag{1}$$

where $\boldsymbol{v}$ is the fluid velocity, ∇ denotes the gradient operator, and $\mu(\dot{\gamma})$ is the effective viscosity depending on the scalar measure $\dot{\gamma}$ of the strain-rate tensor

$$\dot{\gamma} = |2\boldsymbol{E}| = \sqrt{2\,\text{tr}\left(\boldsymbol{E}^T\boldsymbol{E}\right)} = \sqrt{2\,I_2}, \tag{2}$$

with I_2 being the second principal trace of the infinitesimal strain-rate tensor [5,27,28]. Regarding GNFs that exhibit a shear-thinning behaviour and addressing the 5-parameters BCCY rheological formulation, the effective viscosity in Eq. (1) may be described as [5,15]

$$\mu(\dot{\gamma}) = \mu_\infty + \frac{\mu_0 - \mu_\infty}{\left[1 + (\lambda\dot{\gamma})^a\right]^{\frac{1-n}{a}}}, \tag{3}$$

where μ_0 and μ_∞ (with $\mu_\infty < \mu_0$) are the zero-shear rate viscosity and the infinity-shear rate viscosity values (measured in [Pa s]) attained for very low and very high shear rate levels, respectively, λ (measured in [s]) is a characteristic timescale inversely proportional to the shear rate threshold marking the onset of significant shear-thinning effects [9,26], a is a dimensionless strictly-positive model parameter (generally greater than 1), also referred to as the Yasuda parameter [15] and which adjusts the transition between quasi-Newtonian regimes and the dominant shear-thinning response, and n is a dimensionless index regulating the corresponding shear-thinning rate, such that $n \in (0, 1)$.

Referring to the example case shown in Fig. 1, the behaviour captured by the BCCY model is quantitatively consistent with typical experimental observations for many GNFs exhibiting shear-thinning responses [8,18,29,30] and is characterized by:

- a quasi-Newtonian regime at low shear rates (namely, for $\dot{\gamma} \ll 1/\lambda$), associated to a quasi-constant viscosity value $\mu \simeq \mu_0$;
- a strongly nonlinear shear-thinning response for intermediate shear rates (i.e., for $\dot{\gamma} > 1/\lambda$);

- a quasi-Newtonian regime at high shear rates (namely, for $\dot{\gamma} \gg 1/\lambda$), associated to the asymptotic viscosity value μ_∞.

The range of shear rates where the fluid experiences a significant shear-thinning response is usually addressed as power-law region, since it can be effectively described by means of the Ostwald–de Waele power-law relationship [10,11]. In this case, it is possible to assume that $\tau = K\dot{\gamma}^N$, where τ is a scalar measure of the shear stress, K (measured in [Pa s^N]) is the so-called consistency index (with $K > 0$), and N is the dimensionless power-law index. Accordingly, the effective viscosity can be expressed as $\mu(\dot{\gamma}) = \tau/\dot{\gamma} = K\dot{\gamma}^{N-1}$, corresponding to a straight line representation in a log–log graph: $\log_{10} K$ being the intercept of this line with the two axes, and the power-law index N defining the line slope, equal to $N-1$. Consequently, a shear-thinning response is recovered by prescribing $N \in (0,1)$. If outside from the power-law region the fluid is approximated as perfectly Newtonian, the viscosity dependency on the shear rate may be described via a power-law-based piecewise approximation (PWA), resulting in

$$\mu(\dot{\gamma}) = \begin{cases} \mu_0 & \text{for } \dot{\gamma} \le 1/\lambda_0 \\ K\dot{\gamma}^{N-1} & \text{for } 1/\lambda_0 \le \dot{\gamma} \le 1/\lambda_\infty \\ \mu_\infty & \text{for } \dot{\gamma} \ge 1/\lambda_\infty \end{cases}, \tag{4}$$

where the continuous but sharp transitions between ideal Newtonian regimes and the shear-thinning region are identified by the time constants λ_∞ and λ_0 (with $\lambda_\infty < \lambda_0$). It is worth observing that the definition of a PWA needs the setting of four model parameters $(\mu_0, \lambda_0, N, \lambda_\infty)$ that, since the continuity requirement at the characteristic shear rates $\dot{\gamma} = 1/\lambda_0$ and $\dot{\gamma} = 1/\lambda_\infty$, have to satisfy the following relationships

$$K = \mu_0 \lambda_0^{N-1} = \mu_\infty \lambda_\infty^{N-1}, \qquad \frac{\mu_0}{\mu_\infty} = \left(\frac{\lambda_\infty}{\lambda_0}\right)^{N-1}. \tag{5}$$

A possible point of confusion might be how to introduce a PWA of the BCCY model. To this end, assuming the same values for μ_0 and μ_∞ in both the descriptions, as well as $\lambda_0 = \lambda$, can be clearly considered as consistent choices. Accordingly, for a given value of N, the consistency index K and the time constant λ_∞ directly follow from Eqs. (5). But what about the value for the power-law index N? A possible direct choice might be to prescribe that the power-law index N coincides with the BCCY model parameter n [31]. Such an assumption is often implicitly enforced as a consequence of (or justifying) the usually-adopted misleading notation, where the same symbol is generally used to indicate both N and n [4,5,16,25,28]. In the following, the PWA defined by enforcing $N = n$ will be denoted as PWA$_{\text{BCCY}}$.

Referring to the example case introduced in Fig. 1, the comparison between the behaviour predicted by the BCCY model and the corresponding PWA$_{\text{BCCY}}$ highlights that:

- the PWA$_{\text{BCCY}}$ and the BCCY descriptions are in good agreement in representing the onset of the nonlinear shear-thinning response at $\dot{\gamma} \simeq 1/\lambda$;
- for $\dot{\gamma} > 1/\lambda$, the PWA$_{\text{BCCY}}$ exhibits a slope that significantly differs from the local BCCY slope across much of the power-law region;
- the nonlinear shear-thinning regime described by the BCCY model extends well beyond $\dot{\gamma} = 1/\lambda_\infty$, where the PWA$_{\text{BCCY}}$ reaches the lower-bound viscosity value μ_∞.

The discrepancies revealed between BCCY and PWA$_{\text{BCCY}}$ stem from the fact that the BCCY model parameter n in Eq. (3) does not directly correspond to the power-law index N used in the power-law description. Specifically, denoting by n' the slope of the shear stress versus the shear rate in a log–log plot (namely, $n' = d(\log_{10}\tau)/d(\log_{10}\dot{\gamma})$) and focusing on the shear-thinning region, it is evident that n'_{PWA} remains constant and equals N, while n'_{BCCY} varies with the shear rate and cannot be directly expressed solely in terms of n. Consequently, when experimental data are fitted by using the BCCY model, the fitting value for n should not be considered as representative of the power-law index N. Similarly, if the experimental shear-thinning regime is fitted by using the Ostwald–de Waele power-law relationship, the BCCY model defined by assuming $n = N$ may not generally provide a good fit, as specifically addressed in Section 4.

This observation is formally supported by calculating the local slope $S_{\text{BCCY}} = (n'_{\text{BCCY}} - 1)$ of the BCCY viscosity model in a log–log representation and normalized with respect to the power-law viscosity slope $(N-1)$. In detail, by referring to Eq. (3), it results in

$$S_{\text{BCCY}} = \frac{n'_{\text{BCCY}} - 1}{N-1} = \frac{1}{N-1}\frac{d(\log_{10}\mu)}{d(\log_{10}\dot{\gamma})} = \frac{n-1}{N-1}\frac{(\mu_0-\mu_\infty)(\lambda\dot{\gamma})^a}{\mu_\infty\left[1+(\lambda\dot{\gamma})^a\right]^{1+\beta} + (\mu_0-\mu_\infty)\left[1+(\lambda\dot{\gamma})^a\right]}, \tag{6}$$

where $\beta = \left(\frac{1-n}{a}\right) \in (0,1)$. It is simple to prove that Eq. (6) specialized to the case $n = N$ implies the following inequality (see Appendix)

$$0 < S_{\text{BCCY}}\big|_{n=N} < \frac{1-\mu_\infty/\mu_0}{1+\mu_\infty/\mu_0\left[(1+\beta)^{1+\beta}/\beta^\beta - 1\right]} \equiv \mathcal{U} < 1. \tag{7}$$

As a result, the dimensionless upper bound $\mathcal{U}$ decreases as the ratio μ_∞/μ_0 increases, becoming significantly smaller than one within the admissible range of β. This is clearly illustrated in Fig. 2, where $\mathcal{U}$ is plotted against β for different values of the ratio μ_∞/μ_0. For completeness and referring to the example case addressed in Fig. 1, the normalized BCCY slope $S_{\text{BCCY}}|_{N=n}$ introduced in Eq. (6) is also shown, revealing that the discrepancy between the local BCCY slope and the power-law one is always greater than 23%, resulting $S_{\text{BCCY}}|_{n=N} \le 0.77 < \overline{\mathcal{U}} \simeq 0.83$, $\overline{\mathcal{U}}$ being the corresponding value of $\mathcal{U}$.

Therefore, the local slope of the BCCY-based behaviour in a log–log representation does not accurately represent the slope of a power-law description based on the BCCY model parameters, except in the limiting case $\mu_\infty/\mu_0 \to 0^+$. In particular, the indices n in Eq. (3) and N in Eq. (4) have different meanings, and assuming the same value for them is not consistent. This issue can lead to a misleading physical interpretation of results obtained using the BCCY model, and may pose a significant challenge for BCCY model parameter identifiability when combined with power-law approximations.

3. A novel shear-based rheological description

In order to overcome the issues associated to the BCCY model and discussed before, a novel heuristic rheological description is herein proposed.

The rationale arises from the observation that the viscosity function $\mu(\dot{\gamma})$ in GNFs can be thought as the transfer function between the shear stress scalar measure τ and the applied shear rate $\dot{\gamma}$, the corresponding PWA being the asymptotic description of the Bode-like diagram. Such a transfer function, in agreement with both the previously-recalled physical evidence for shear-thinning inelastic fluids and basic concepts of the control theory, has to be characterized by the static gain μ_0, and by the presence of both a pole and a zero, each with a multiplicity of one. Specifically, the pole corresponds to the characteristic shear rate level $\dot{\gamma}_0 = 1/\lambda_0$, which marks the decrease onset of μ from μ_0; the zero is associated to the characteristic shear rate level $\dot{\gamma}_\infty = 1/\lambda_\infty$ beyond which μ stabilizes towards the constant value μ_∞. Accordingly, the following rheological model is proposed:

$$\mu(\dot{\gamma}) = \mu_0\left[\frac{1+\left(\lambda_\infty\dot{\gamma}\right)^\alpha}{1+\left(\lambda_0\dot{\gamma}\right)^\alpha}\right]^{\frac{1-\eta}{\alpha}}. \tag{8}$$

This description involves five parameters: μ_0, λ_0, λ_∞, and the positive dimensionless quantities α and η, which have meanings formally equivalent to those of a and n, respectively, in Eq. (3). Thereby, when $\lambda_\infty < \lambda_0$ and $\alpha > 1$, a shear-thinning behaviour is obtained if $\eta \in (0,1)$.

It is worth noticing that, with respect to the BCCY model, the rheological description in Eq. (8) emphasizes the role of the time

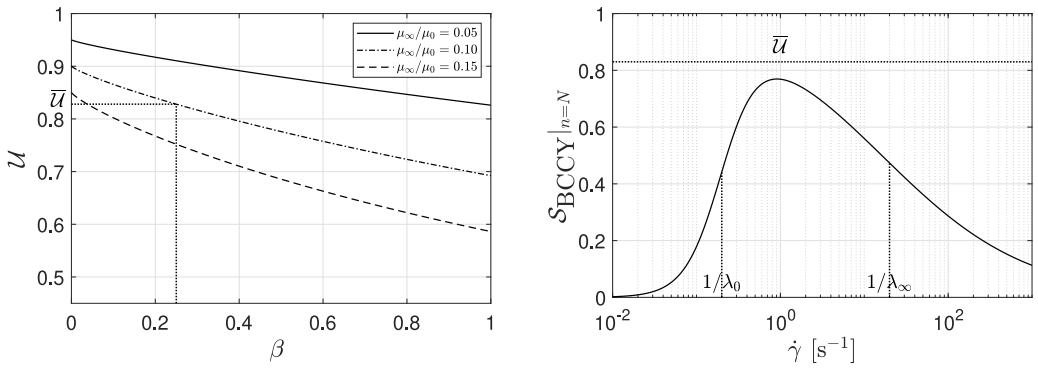

Fig. 2. Case $n = N$. (a) Upper bound $\mathcal{U}$ introduced in Eq. (7) versus $\beta = (1-n)/a$ and for different values of the ratio μ_∞/μ_0. The quantity $\overline{\mathcal{U}}$ identifies the value of $\mathcal{U}$ corresponding to the example case introduced in Fig. 1 (i.e., for $\beta = 0.25$ and $\mu_\infty/\mu_0 = 0.1$). (b) Shear rate dependency of the normalized BCCY slope $\mathcal{S}_{\mathrm{BCCY}}|_{n=N}$ for the example case in Fig. 1.

constant λ_∞ as an independent parameter instead of μ_∞, this latter simply resulting for $\dot{\gamma} \to +\infty$ from

$$\mu_\infty = \mu_0 \left(\frac{\lambda_\infty}{\lambda_0}\right)^{1-\eta} . \tag{9}$$

In other words, dominant features of the shear-thinning response are assumed to be associated to the characteristic shear rate levels $\dot{\gamma}_0 = 1/\lambda_0$ and $\dot{\gamma}_\infty = 1/\lambda_\infty$, that identify the shear rate range in which the highly non-Newtonian response occurs, rather than the asymptotic viscosity value associated to the quasi-Newtonian regime. For this reason the rheological description in Eq. (8) will be denoted in the following as shear rate-based model (SRB).

The proposed model is able to recover two other possible rheological shear-thinning responses:

- In the limit for $\lambda_\infty \to 0^+$, Eq. (8) reduces to

$$\mu(\dot{\gamma}) = \frac{\mu_0}{\left[1 + \left(\lambda_0\dot{\gamma}\right)^\alpha\right]^{\frac{1-\eta}{\alpha}}} , \tag{10}$$

  that corresponds to the Yasuda model [15], or equivalently to the limit condition associated to the BCCY model for $\mu_\infty \to 0^+$. This response is representative of a quasi-Newtonian regime characterized by $\mu \simeq \mu_0$ for small shear rates (i.e., for $\dot{\gamma} < 1/\lambda_0$), followed by an indefinite shear-thinning behaviour for any value of the shear rate greater than $1/\lambda_0$.
- In the limit for $\lambda_0 \to +\infty$, and accounting for Eq. (9), Eq. (8) reduces to

$$\mu(\dot{\gamma}) = \frac{K}{\dot{\gamma}^{1-\eta}} \left[1 + \left(\lambda_\infty\dot{\gamma}\right)^\alpha\right]^{\frac{(1-\eta)}{\alpha}} , \tag{11}$$

  with $K = \mu_\infty \lambda_\infty^{\eta-1}$, which describes a shear-thinning behaviour for shear rates lower than $1/\lambda_\infty$ (with a viscosity singularity at $\dot{\gamma} = 0$), followed by a quasi-Newtonian regime characterized by $\mu \simeq \mu_\infty$ for $\dot{\gamma} > 1/\lambda_\infty$.

It is important to emphasize that the model parameter η introduced in Eq. (8) furnishes, in comparison with n in the BCCY description, a more effective representation of the power-lax index N associated with a SRB-based PWA. As a matter of fact, the local slope $\mathcal{S}_{\mathrm{SRB}} = (n'_{\mathrm{SRB}} - 1)$ of the SRB viscosity model in a log–log representation and normalized with respect to the power-law viscosity slope $(N-1)$, is

$$\mathcal{S}_{\mathrm{SRB}} = \frac{n'_{\mathrm{SRB}} - 1}{N-1} = \frac{1}{N-1}\frac{d(\log_{10}\mu)}{d(\log_{10}\dot{\gamma})} = \frac{\eta-1}{N-1}\frac{\dot{\gamma}^a\left(\lambda_0^a - \lambda_\infty^a\right)}{\left[1+\left(\lambda_0\dot{\gamma}\right)^a\right]\left[1+\left(\lambda_\infty\dot{\gamma}\right)^a\right]} . \tag{12}$$

In order to perform a consistent comparison among the BCCY, PWA and SRB descriptions, from now on μ_0 and μ_∞ are assumed to have the same values in all the models, and the other parameters are assumed to satisfy the following consistency conditions (see Eq. (9)): $\alpha = a$, $\lambda_0 = \lambda$, $\lambda_\infty = \lambda_0(\mu_\infty/\mu_0)^{1/(1-\eta)}$, $\eta = n = N$. In this case, it can be shown that (see Appendix)

$$0 < \mathcal{S}_{\mathrm{BCCY}} < \mathcal{S}_{\mathrm{SRB}} < (\mathcal{S}_{\mathrm{SRB}})_{max} < 1 \qquad \text{for} \quad \frac{1}{\lambda_0} < \dot{\gamma} < \frac{1}{\lambda_\infty} , \tag{13}$$

where

$$(\mathcal{S}_{\mathrm{SRB}})_{max} = \frac{\lambda_0^{a/2} - \lambda_\infty^{a/2}}{\lambda_0^{a/2} + \lambda_\infty^{a/2}} \tag{14}$$

is the maximum value of the shear rate function $\mathcal{S}_{\mathrm{SRB}}$ attained at $\dot{\gamma}_{max} = (\lambda_0\lambda_\infty)^{-a/2} \in (1/\lambda_0, 1/\lambda_\infty)$.

In this case and for different choices of model parameters, Fig. 3 clearly highlights that the SRB slope is significantly closer to the power-law one within the overall shear-thinning regime than the BCCY case. Accordingly, the model parameter η introduced in the SRB description is expected to be much more representative of the power-law index associated to a power-law-based approximation than the corresponding parameter n appearing in the BCCY model. This is clearly confirmed by analysing Fig. 4 where, for different values of $\eta = N$, the nonlinear responses experienced by considering PWA and SRB descriptions are in a very good agreement each other, whereas the BCCY model defined by considering $n = N$ significantly deviates from them within the shear-thinning region.

4. Model parameter identifiability and flow description

To highlight the parameter identifiability issues associated with the BCCY model and to demonstrate the superior identifiability performance of the proposed SRB description, direct and inverse estimation procedures based on available experimental measurements are presented. Specifically, reference is made to the experimental viscosity data obtained by Colosi et al. [32] for a cell-laden hydrogel, which exhibits a typical shear-thinning response, that is a decreasing shear rate dependency of viscosity. For the sake of simplicity, the model parameters α (for SRB) and a (for BCCY) are assumed to be equal, and characterized by the a-priori fixed value $\alpha = a = 2$ which gives accurate fits for many polymeric fluids and melts [5,28]. Finally, the performance of both rheological models in capturing the flow properties of a representative shear-thinning fluid is briefly discussed. Specifically, in order to clearly highlight the descriptive capability of the models, independent of possible effects related to the specificity of the application, reference is made to the simple case of a steady flow in a cylindrical channel.

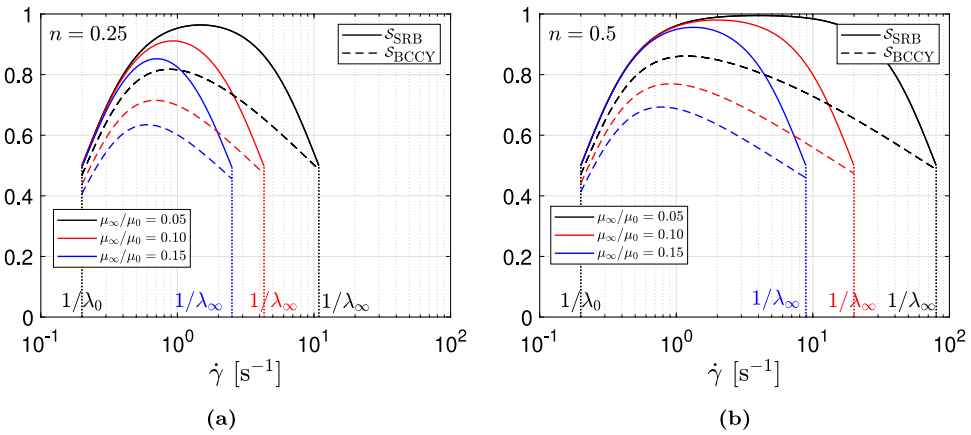

Fig. 3. Shear rate dependency of local normalized slopes S_{BCCY} (dashed lines) and S_{SRB} (continuous lines) introduced in Eqs. (6) and (12), respectively. Values of model parameters: $\alpha = a = 2$, $\lambda_0 = \lambda = 5$ s, $\lambda_\infty = \lambda_0(\mu_\infty/\mu_0)^{1/(1-\eta)}$, $\eta = n = N$. (a) Case $n = 0.25$. (b) Case $n = 0.5$.

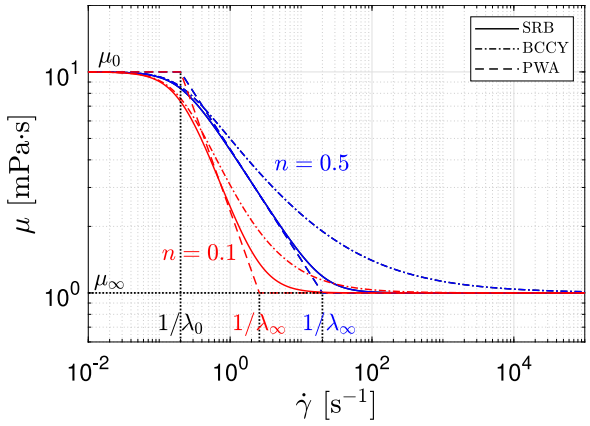

Fig. 4. Shear-thinning response associated to SRB, BCCY and PWA descriptions and by assuming $\eta = n = N$, $\lambda_0 = \lambda$, $\lambda_\infty = \lambda_0(\mu_\infty/\mu_0)^{1/(1-\eta)}$, $K = \mu_0\lambda_0^{\eta-1}$. Values of model parameters: $\mu_0 = 10$ mPa s, $\mu_\infty = 1$ mPa s, $\lambda_0 = 5$ s, $a = 2$, $n = 0.5$ (blue), $n = 0.1$ (red).

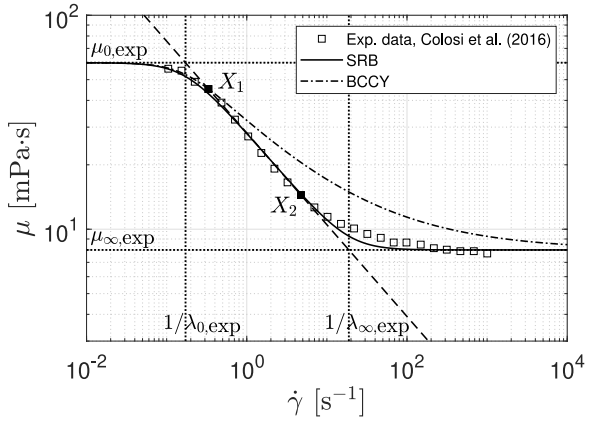

Fig. 5. Direct parameter estimation based on a straightforward heuristic visual fitting of the experimental data reported in [32]. Comparison between the corresponding SRB and BCCY rheological descriptions, defined by the experimentally-derived model parameters summarized in Table 1 ($a = \alpha = 2$, $n = \eta = N_{exp}$, $\lambda = \lambda_{0,exp}$).

4.1. Direct parameter estimation from experimental data

Parameters for both the BCCY and the SRB models are initially identified by using a direct estimation procedure from experimental data, without employing iterative approaches based on nonlinear regression techniques. Specifically, Fig. 5 shows the experimental data (represented by square symbols) as represented via a log–log plot in the plane $(\dot{\gamma}, \mu)$. The adopted direct estimation procedure is defined by the following steps:

- Identification of asymptotic viscosity values. The experimental estimates for the asymptotic viscosity values, denoted as $\mu_{0,exp}$ and $\mu_{\infty,exp}$ are assumed to approximate the largest and smallest viscosity experimental measurements, respectively. In Fig. 5, $\mu_{0,exp}$ and $\mu_{\infty,exp}$ are represented by horizontal dot lines.
- Identification of the power-law region. The power-law region is identified by considering the portion of the experimental data that in the log–log plot exhibits a linear trend. In the case under consideration (Fig. 5), such a linear trend is described through the straight dashed line passing through the experimental data points $X_1 \equiv (\dot{\gamma}_1, \mu_1)$ and $X_2 \equiv (\dot{\gamma}_2, \mu_2)$. Accordingly, the experimentally-deduced power-law parameters, namely the consistency index K and the dimensionless power-law index N, straightly result from

$$K^*_{exp} = \frac{\mu^*_1\dot{\gamma}^*_2 - \mu^*_2\dot{\gamma}^*_1}{\dot{\gamma}^*_2 - \dot{\gamma}^*_1}, \qquad N_{exp} = 1 - \frac{\mu^*_1 - \mu^*_2}{\dot{\gamma}^*_2 - \dot{\gamma}^*_1}, \tag{15}$$

  where $q^* = \log_{10} q$.
- Determination of time constants. Since Eqs. (5), the experimentally-based time constants $\lambda_{0,exp}$ and $\lambda_{\infty,exp}$ are determined as follows:

$$\lambda_{0,exp} = \left(\frac{K_{exp}}{\mu_{0,exp}}\right)^{\frac{1}{N_{exp}}-1}, \qquad \lambda_{\infty,exp} = \left(\frac{K_{exp}}{\mu_{\infty,exp}}\right)^{\frac{1}{N_{exp}}-1}. \tag{16}$$

  The inverses of these constants correspond to the characteristic shear rate levels at which the power-law dashed line in Fig. 5 intersects the two horizontal dotted lines representing the asymptotic viscosity values.

The values of model parameters derived from the experimental viscosity data through the described direct identification procedure are reported in Table 1. Assuming $n = \eta = N_{exp}$ and $\lambda = \lambda_{0,exp}$, Fig. 5 represents a comparison between the rheological responses obtained from the BCCY and SRB descriptions. As it clearly appears, the SRB model demonstrates excellent fitting capability, whereas the BCCY model provides a good fit only in the transition region at $\dot{\gamma} \simeq 1/\lambda_{0,exp}$, failing to accurately capture the experimental behaviour in the power-law region and the transition towards the asymptotic quasi-Newtonian response at $\mu \simeq \mu_{\infty,exp}$.

Accordingly, the herein-described simple direct estimation procedure provides an effective and accurate SRB-based rheological description. However, it proves insufficient for the BCCY model, which requires an inverse identification procedure based on nonlinear regression techniques, as discussed in the following.

Table 1
Values of model parameters derived through the direct estimation procedure from the experimental data reported in [32].

$\mu_{0,\text{exp}}$ [mPa s]	$\mu_{\infty,\text{exp}}$ [mPa s]	K_{exp} [mPa s^N]	N_{exp} [−]	$\lambda_{0,\text{exp}}$ [s]	$\lambda_{\infty,\text{exp}}$ [s]
60.0	8.0	28.2	0.571	5.812	0.053

4.2. Inverse parameter identification through a nonlinear regression technique

Model parameter estimation is now carried out through a nonlinear regression procedure based on the maximum likelihood estimation method [33,34].

Due to the nonlinearity of the models under investigation, parameter identification may depend on both the choice of data representation and the definition of the loss function [35–37]. In this study, to enhance fitting performance and enable meaningful model comparison, a log–log data representation is adopted, and the lognormal mean absolute percentage error (LMAPE) is used as the loss function in place of the conventional sum of squared errors. Specifically, the optimization problem aims to determine the set of model parameters that minimizes the LMAPE, defined as:

$$\text{LMAPE} = \frac{1}{T}\sum_{i=1}^{T}\left|\frac{\log f_i}{\log b_i} - 1\right|, \tag{17}$$

where the logarithm operator is taken to base 10, T is the number of experimental measurements, b_i denotes the i-th measured viscosity value, and f_i represents the corresponding prediction provided by the rheological model.

In addition, the coefficient of determination R^2 is employed as a supplementary metric for model comparison. In the context of nonlinear regression, its definition can be adapted to the specific case in order to provide a quantitative measure of goodness of fit [34,38,39]. In this study, the coefficient of determination is defined as:

$$R^2_{\text{LMAPE}} = 1 - \frac{\text{LMAPE}}{\frac{1}{T}\sum_{i=1}^{T}\left|\frac{\bar{y}_L}{\log b_i} - 1\right|}, \tag{18}$$

where $\bar{y}_L = (\sum_{i=1}^{T}\log b_i)/T$ represents the mean logarithmic experimental value. A value of R^2_{LMAPE} close to one indicates that the rheological model closely fits the experimental data, while a value approaching zero suggests poor model accuracy [33,34].

Furthermore, to provide a more meaningful assessment of the goodness of fit in the context of nonlinear regression, the reduced chi-square statistic $\bar{\chi}^2$ is also employed as an additional goodness-of-fit metric [40]. It is defined as:

$$\bar{\chi}^2 = \frac{\chi^2}{\text{DoF}} = \frac{1}{\text{DoF}}\sum_{i=1}^{T}\left(\frac{f_i - b_i}{\sigma_i}\right)^2, \tag{19}$$

where $\text{DoF} = (T - \#\mathcal{P})$ is the number of degrees of freedom, $\#\mathcal{P}$ denotes the number of model parameters, and σ_i is the standard deviation associated with the ith viscosity measurement. Specifically, a value of $\bar{\chi}^2 \approx 1$ indicates a good fit; values significantly larger than one suggest a poor fit, while values much smaller than one may imply potential overfitting (i.e., the model also captures random noise in the data) [41,42]. Since the experimental data in [32] do not report values of σ_i they are assumed, in agreement with [40,43], to be 5% of the corresponding measured values b_i, for the sake of consistent model comparison.

As a result of an iterative numerical procedure implemented in the MATLAB environment (R2024b, MathWorks, MA, USA), Table 2 summarizes the optimal parameter values computed for both the BCCY and SRB models. It is worth noting that, in accordance with the considerations presented in Sections 2 and 3, the parameter λ_∞ does not explicitly appears in the BCCY formulation, but is instead derived from Eqs. (5) once μ_0, λ, n, and μ_∞ are determined. Conversely, λ_∞ directly appears in the SRB model introduced in Eq. (8), while μ_∞ is derived from Eq. (9). Therefore, the parameters (μ_0, λ, n, μ_∞) for the BCCY model and (μ_0, λ_0, η, λ_∞) for the SRB model are denoted as primary parameters, while λ_∞ for the BCCY and μ_∞ for the SRB model are referred to as derived parameters.

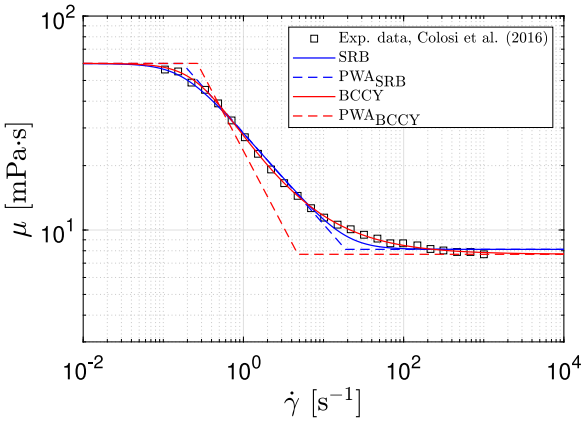

Fig. 6. Inverse identification of model parameters through numerical nonlinear regression. Comparison of the fitting performance of the SRB and BCCY models, along with their corresponding piecewise approximations (PWA$_{\text{SRB}}$ and PWA$_{\text{BCCY}}$). The optimal values of the model parameters are summarized in Table 2.

For completeness, Table 2 also reports the optimal LMAPE values along with the corresponding values for the coefficient of determination R^2_{LMAPE} and the reduced chi-square $\bar{\chi}^2$.

Specifically, the minimum LMAPE value obtained by the optimization procedure for the SRB model is slightly higher than that of the BCCY model. Consequently, the coefficient of determination R^2_{LMAPE} for the SRB model is marginally lower than that for the BCCY formulation. Accordingly, this outcome suggests that, based on the computed optimal parameter sets, the BCCY model provides a slightly better fit to the experimental data compared to the SRB model. Nevertheless, the latter still exhibits very good fitting performance, as clearly illustrated in Fig. 6, where the experimental data from Colosi et al. [32] are well fitted by both the SRB and BCCY models optimized through the numerical nonlinear regression.

On the other hand, the computed values of the reduced chi-square $\bar{\chi}^2$ differ significantly, resulting in $\bar{\chi}^2 \approx 1$ for the SRB model and $\bar{\chi}^2 < 0.1$ for the BCCY one. Such a result confirms the good fitting performance of the SRB model, while also highlights a clear tendency of the BCCY model to suffer from potential overfitting.

The comparison between the values summarized in Table 2 and those reported in Table 1 reveals that the BCCY optimal parameters significantly differ from those obtained through the simple direct estimation procedure described in Section 4.1. In contrast, the direct identification procedure, based on a straightforward heuristic visual fitting approach, yields an estimation for the SRB model parameters that closely matches the optimal one numerically obtained via the iterative nonlinear regression strategy.

Let the power-law-based piecewise approximations PWA$_{\text{SRB}}$ and PWA$_{\text{BCCY}}$ be considered (see Eq. (4)), built up with the inverse identification results associated with the SRB and BCCY descriptions, respectively. As shown in the comparison presented in Fig. 6, PWA$_{\text{BCCY}}$, despite being based on optimal parameters that ensure the best fit for the BCCY description, fails to effectively capture the experimental response. In contrast, PWA$_{\text{SRB}}$ exhibits an excellent agreement with

Table 2
Inverse identification of model parameters for SRB and BCCY rheological descriptions performed via a nonlinear regression procedure based on the maximum likelihood estimation method. Primary and derived (underlined) fitting values ($a = \alpha = 2$, $n^* = \eta$ and $\lambda^* = \lambda_0$ for SRB; $n^* = n$ and $\lambda^* = \lambda$ for BCCY).

	μ_0 [mPa s]	μ_∞ [mPa s]	λ^* [s]	λ_∞ [s]	n^* [−]	LMAPE [−]	R^2_{LMAPE} [−]	$\bar{\chi}^2$ [−]
SRB	60.0	<u>8.14</u>	5.747	0.053	0.573	0.0155	0.93	0.96
BCCY	60.1	7.70	3.759	<u>0.209</u>	0.289	0.0034	0.98	0.09

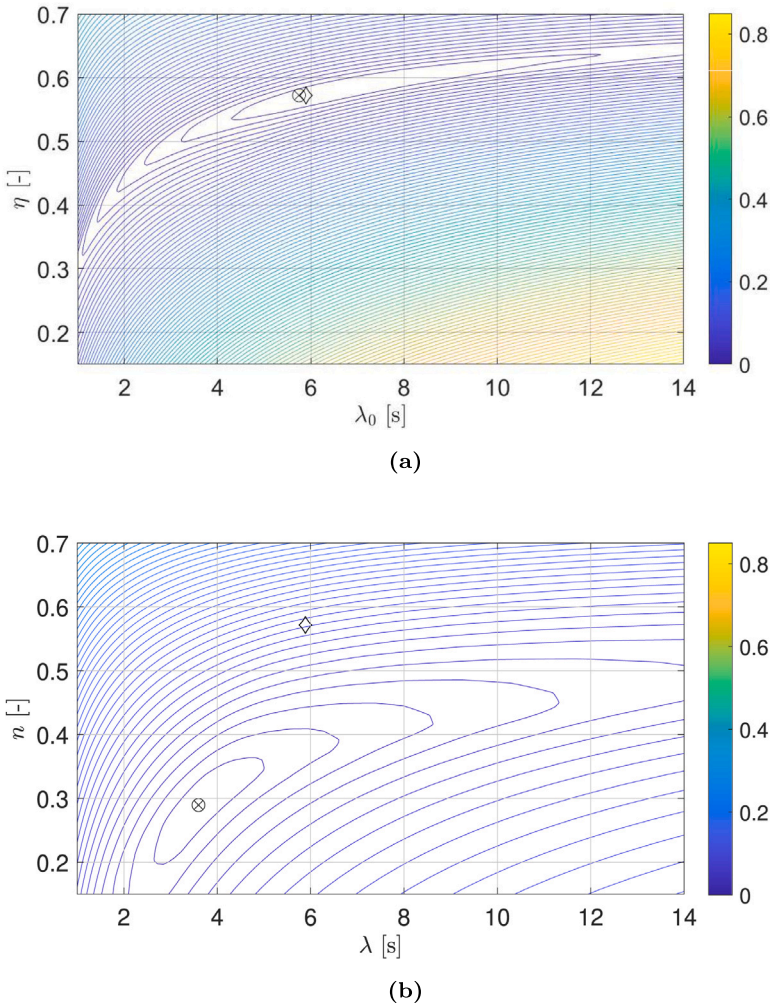

Fig. 7. Isolines of the likelihood surface $\mathcal{L}(\lambda^*, n^*)$ introduced in Eq. (20) ($n^* = \eta$ and $\lambda^* = \lambda_0$ for SRB; $n^* = n$ and $\lambda^* = \lambda$ for BCCY). Model parameters different from λ^* and n^* are held fixed and equal to the optimal values summarized in Table 2. (a) SRB model: $\mathcal{L}(\lambda_0, \eta)$; (b) BCCY model: $\mathcal{L}(\lambda, n)$. ⊗: optimality condition computed via the inverse identification strategy; ◇: direct estimation state.

the experimental data, accurately reproducing both the power-law behaviour and the transition phases toward quasi-Newtonian regimes.

This result provides further compelling evidence of a critical identifiability issue associated with the BCCY description, arising from the fact that the BCCY model parameter n in Eq. (3) ($n = 0.289$ at the optimality condition) does not directly correspond to the power-law index N used in the power-law description. Instead, the proposed results confirm that the power-law index N is more accurately represented by the SRB model parameter η in Eq. (8) ($\eta = 0.573$ at the optimality condition).

Finally, to demonstrate the greater robustness of the proposed SRB model in terms of identifiability features, particularly in comparison to the BCCY model, the variability of LMAPE associated to deviations of model parameters from the optimality condition is analysed. For the sake of simplicity, reference is made to λ^* and n^* only ($n^* = \eta$ and $\lambda^* = \lambda_0$ for SRB; $n^* = n$ and $\lambda^* = \lambda$ for BCCY), as these primary parameters play a key role in capturing the onset and evolution of the nonlinear shear-thinning response. Specifically, let the likelihood function $\mathcal{L}$ be defined as

$$\mathcal{L}(\lambda^*, n^*) = \text{LMAPE}(\lambda^*, n^*, \hat{\mathcal{P}}), \tag{20}$$

where $\hat{\mathcal{P}}$ denotes the set of primary model parameters complementary to λ^* and n^*, which are held fixed at their optimal values (see Table 2). Fig. 7 presents the isolines of the likelihood surface $\mathcal{L}(\lambda^*, n^*)$ obtained for the SRB and BCCY descriptions, highlighting how LMAPE varies from its optimal value when only λ^* and n^* vary. For completeness, the result of the direct estimation procedure from experimental data is also indicated. Once again, it clearly appears that in the case of the SRB model the inverse and the direct estimation procedures give very close results, differently from the case of the BCCY description. Furthermore, the analysis of the isolines of $\mathcal{L}(\lambda, n)$ obtained for the BCCY model (Fig. 7b) confirms the findings provided by Gallagher et al. [16]. As a matter

Table 3
Primary and derived (underlined) fitting values of model parameters, obtained through the inverse identification procedure and based on synthetic data reported in Fig. 8 ($a = \alpha = 2$, $n^* = \eta$ and $\lambda^* = \lambda_0$ for SRB; $n^* = n$ and $\lambda^* = \lambda$ for BCCY).

	μ_0 [mPa s]	μ_∞ [mPa s]	λ^* [s]	λ_∞ [s]	n^* [−]
SRB	60.0	<u>8.14</u>	$9.58 \cdot 10^{-2}$	$8.86 \cdot 10^{-4}$	0.573
BCCY	60.1	7.00	$6.25 \cdot 10^{-2}$	<u>$4.24 \cdot 10^{-3}$</u>	0.300

of fact, the BCCY likelihood surface exhibits a large flat region around the optimality condition. Consequently, significant variations of model parameters λ and n can marginally affect the fitting of the experimental data, but they can lead to very different flow dynamics (as discussed in the following), making these parameters unreliable for inferring the physical properties of the investigated fluid.

By contrast, this identifiability issue is substantially mitigated in the proposed SRB model. The corresponding likelihood surface exhibits steep gradients around the optimal condition, indicating that even small perturbations in λ_0 and η result in significant variations in $\mathcal{L}(\lambda_0, \eta)$. Consequently, minor changes in the primary parameters can noticeably affect the fit performance of the model against the experimental data. This behaviour, combined with the fact that the SRB model parameters can be effectively estimated through a direct approach, underscores its superior identifiability properties, making it a more effective and robust alternative to the BCCY formulation.

4.3. A representative case of flow description

To further emphasize the previously stated observations regarding the impact of potential identifiability issues on the flow description of generalized Newtonian fluids, reference is made to the simple case of a steady flow in a pipe involving an exemplary shear-thinning incompressible fluid. This case can be considered representative of an extrusion-based bioprinting process [44–46]. In particular, a cylindrical nozzle is examined, where R denotes the cross-sectional radius and L the axial length (i.e., along the coordinate z). Accordingly, the steady flow is fully described by the following axisymmetric one-dimensional problem [5,46]:

$$\begin{aligned} &\frac{1}{r}\frac{d}{dr}\left[r\mu(\dot\gamma)\frac{dv_z}{dr}\right] + \frac{\Delta p}{L} = 0 && \text{for } r \in [0, R] \\ &\frac{dv_z}{dr} = 0 && \text{at } r = 0 \\ &v_z = 0 && \text{at } r = R \end{aligned} \tag{21}$$

where $\Delta p/L = -dp/dz$ is the constant axial pressure gradient, $v_z = v_z(r)$ is the axial velocity component (the only non-zero component), r is the radial coordinate, and $\dot\gamma$ is the scalar shear rate measure, given by $\dot\gamma = |dv_z/dr|$.

The rheological description of the exemplary fluid has been defined considering a set of 50 synthetic data points representing a typical shear-thinning behaviour, and generated from the BCCY model with the addition of small lognormal noise (standard deviation 0.018), as shown in Fig. 8. The model parameters resulting from the numerical inverse identification procedure introduced in Section 4.2 are summarized in Table 3 for both SRB and BCCY. The corresponding rheological predictions are compared in Fig. 8. Furthermore, Fig. 8 illustrates the rheological predictions of both models when a variation in the primary model parameters n^* and λ^* (that is, n and λ for BCCY, and η and λ_0 for SRB) is introduced with respect to the optimality condition. Specifically, n^* is increased by 15%, while λ^* is reduced by 15%, both relative to their optimal values (see Table 3).

Starting from the fluid rheological response, the steady velocity profile can be computed by solving the problem introduced in Eqs. (21). In particular, assuming $\Delta p/L = 175.0$ Pa/mm and $R = 100\,\mu$m, Fig. 9 depicts the velocity profiles associated with both the optimality conditions and the perturbed ones, computed via a numeric finite-difference scheme. Specifically, referring to the optimal parameter values for

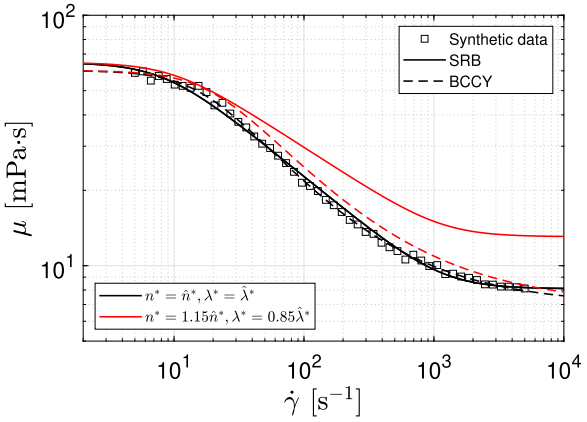

Fig. 8. Rheological response of a representative shear-thinning fluid defined by a set of 50 synthetic data points (square symbols). Optimal fittings (black lines) obtained through the inverse identification procedure for both the SRB (solid line) and BCCY (dashed line) formulations. The optimal model parameter values are summarized in Table 3. Red lines represent the rheological predictions when the primary model parameters n^* and λ^* ($n^* = n$ and $\lambda^* = \lambda$ for BCCY; $n^* = \eta$ and $\lambda^* = \lambda_0$ for SRB) are perturbed with respect to the optimal condition.

the SRB model, the flow solution is characterized by a cross-sectional average velocity of $\bar V \approx 20$ mm/s, corresponding to a flow shear-rate measure $\dot\gamma_F = 2\bar V/R \approx 200$ s^{-1}. The Carreau numbers [25,26], computed with respect to the characteristic shear rates $\dot\gamma_0 = 1/\lambda_0$ and $\dot\gamma_\infty = 1/\lambda_\infty$, are $\mathrm{Cu}_0 = \dot\gamma_F/\dot\gamma_0 = 19.17$ and $\mathrm{Cu}_\infty = \dot\gamma_F/\dot\gamma_\infty = 0.18$, indicating an intermediate shear-thinning regime. Moreover, Fig. 9 also shows the analytical solutions derived by assuming the fluid response in the cylindrical nozzle as completely described by the Ostwald–de Waele power-law model, that is by considering $\mu(\dot\gamma) = K\dot\gamma^{N-1}$. In this case, the velocity profile is analytically represented by [5,46]:

$$v_z(r) = \frac{N}{N+1}\left(\frac{\Delta p}{2LK}\right)^{\frac{1}{N}}\left(R^{\frac{N+1}{N}} - r^{\frac{N+1}{N}}\right), \tag{22}$$

where, accounting for Eq. (5), model parameters K and N are computed via μ_0, λ^* and $N = n^*$ (with $n^* = \eta$ and $\lambda^* = \lambda_0$ for SRB; $n^* = n$ and $\lambda^* = \lambda$ for BCCY) corresponding to the results of the inverse identification procedure (see Table 3).

The proposed results show that:

- The velocity profiles numerically computed using both the SRB and BCCY models under optimal conditions are very similar, with differences of less than 2%. Moreover, both models yield nearly the same cross-section average velocity $\bar V$.
- When model parameters deviate from their optimal values, the BCCY formulation continues to provide a reasonably accurate rheological description compared to the reference data, unlike the SRB formulation (Fig. 8). Specifically, the maximum deviation between BCCY predictions and the reference data remains below 11%, whereas discrepancies in the SRB-based rheological description can exceed 60%.
- Although significant deviations from the optimal model parameters do not substantially affect the rheological response of the BCCY model, the resulting flow description can differ significantly from the actual one (see Fig. 9). Specifically, considerable discrepancies arise when comparing the BCCY-based velocity

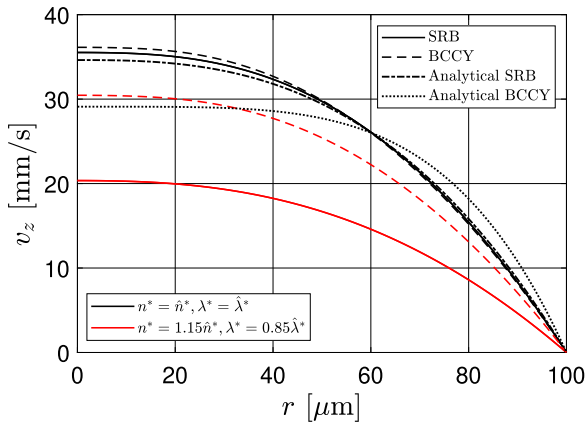

Fig. 9. Prediction of velocity profiles for a steady incompressible flow in a cylindrical channel ($\Delta p/L$ = 175.0 Pa/mm, R = 100 μm) when the rheological shear-thinning response in Fig. 8 is considered. Numerical predictions based on SRB (solid lines) and BCCY (dashed lines) models: comparison between velocity profiles associated with the optimality conditions (black lines) and the perturbed ones (red lines). Power-law-based analytical solution, described by Eq. (22) and obtained via the nonlinear regression results for both SRB and BCCY models, is also reported. The optimal model parameter values are summarized in Table 3.

profiles computed using the optimal and the perturbed parameters, with differences exceeding 17% (approximately 14% in the average velocity value). This evidence further confirms the identifiability issue of the BCCY model, as highlighted by Gallagher et al. [16]. Conversely, since deviations from the optimal parameter values lead to significant changes in the rheological response described by the SRB model (see Fig. 8), the corresponding velocity profiles coherently exhibit significant discrepancies (of approximately 40%).

- The analytical velocity profile in Eq. (22) obtained using the Ostwald–de Waele power-law model based on the SRB nonlinear regression exhibits excellent agreement with the optimal numerical solutions, with differences lower than 4%. In contrast, the power-law analytical profile derived by employing model parameters obtained from the BCCY nonlinear regression shows significant discrepancies compared to the optimal numerical solutions, with differences exceeding 17%. Given the values summarized in Table 3, this finding further confirms that the BCCY model parameter n cannot be directly adopted — or straightforwardly identified — within a power-law description. Conversely, the SRB model parameter η is better suited to approximate the power-law index N. Therefore, the SRB formulation effectively overcomes the critical identifiability issues of the BCCY model, enabling a simple and efficient estimation procedure based on a direct approach.

5. Conclusions

The Carreau–Yasuda model (BCCY) is widely used to describe the shear-thinning behaviour of non-Newtonian inelastic fluids in many research and industrial applications. However, its parameter identification through experimental data fitting is often affected by intrinsic identifiability issues, leading to misleading interpretations of model parameters and unreliable flow predictions. To address these limitations, this paper proposed a novel rheological formulation specifically designed to mitigate such identifiability challenges.

Comparisons based on analytical arguments and numerical assessments demonstrated that the proposed model relies on physically meaningful parameters, whose identifiability is not compromised by the key issues affecting the Carreau–Yasuda formulation. The new approach allows for effective parameter estimation through a straightforward direct identification strategy, eliminating the need for numerical inverse optimization procedures based on nonlinear regression techniques. Moreover, the proposed formulation enables the identication of two Carreau numbers based on the two characteristic shear rates of the fluid.

The results presented in this study highlight that the novel model not only provides a robust and accurate description of shear-thinning fluids but also ensures improved reliability in flow predictions. By addressing the fundamental shortcomings of the BCCY model, this formulation represents a promising alternative for advanced applications requiring precise rheological characterizations.

Future work may include the extension of the analysis to more complex flow conditions, the comparison with other generalized Newtonian fluid (GNF) formulations, and the validation of the model against a broader range of experimental data. In particular, the identifiability properties of the proposed rheological relationship could be further investigated by performing uncertainty quantification on both the rheological parameters and the flow model parameters (e.g., geometry, reference velocity), as carried out by Kim et al. [47] for other GNF models. Moreover, potential applications span various fields, including industrial processes and biomedical systems, with particular relevance to bioprinting technologies [44–46] and the modelling of cell-laden hydrogels [48,49], where accurate prediction of shear-thinning behaviour is critical to preserve cell viability and achieve precise material deposition. The model also holds promise for advanced hemodynamic applications, for instance related to the influence of blood-vessel interaction in health and pathological tissue remodelling [50].

CRediT authorship contribution statement

Gianluca Santesarti: Writing – review & editing, Writing – original draft, Visualization, Software, Methodology, Data curation, Conceptualization. **Michele Marino:** Writing – review & editing, Supervision, Methodology, Conceptualization. **Francesco Viola:** Writing – review & editing, Supervision, Methodology, Conceptualization. **Roberto Verzicco:** Supervision, Methodology, Conceptualization. **Giuseppe Vairo:** Writing – review & editing, Writing – original draft, Supervision, Methodology, Conceptualization.

Declaration of competing interest

The authors declare that they have no known competing financial interests or personal relationships that could have appeared to influence the work reported in this paper.

Acknowledgements

Part of this work was carried out with the support from the Italian National Group for Mathematical Physics GNFM-INdAM.

Giuseppe Vairo acknowledges financial support by the Italian Ministry of University and Research (MUR) under the National Recovery and Resilience Plan (NRRP), within the PRIN 2022 program, Project 2022T3SLAZ, CUP E53D23003700006. Michele Marino acknowledges financial support under the National Recovery and Resilience Plan (NRRP) by the Italian Ministry of University and Research (MUR), funded by the European Union - NextGenerationEU, within the PRIN 2022 program, Project 2022Z24WLR (project acronym: MATERIAL), CUP: E53C24002920006. Franceco Viola acknowledges financial support by the European Research Council (ERC) under the European Union's Horizon Europe research and innovation program, Project CARDIOTRIALS, Grant No. 101039657.

Appendix

Consistently with symbols defined in Sections 2 and 3, and by assuming $\alpha = a$, $\eta = n = N$, $\lambda = \lambda_0$, let the following notation be introduced

$$x = (\lambda_0\dot{\gamma})^a, \qquad \beta = \frac{1-n}{a}, \qquad g = \left(\frac{\lambda_\infty}{\lambda_0}\right)^a, \tag{A.1}$$

so that

$$\mu_\infty/\mu_0 = g^\beta, \qquad 0 < \beta < 1, \qquad 0 < g < g^\beta < 1. \tag{A.2}$$

Thereby, the shear rate range $1/\lambda_0 \le \dot{\gamma} \le 1/\lambda_\infty$, that identifies the shear-thinning region, corresponds to $1 < x < 1/g$. Accordingly, Eqs. (6) and (12) can be recast as

$$S_{\mathrm{BCCY}}(x) = \frac{x(1-g^\beta)}{(1+x)[(1-g^\beta)+g^\beta(1+x)^\beta]}, \tag{A.3}$$

$$S_{\mathrm{SRB}}(x) = \frac{x(1-g)}{(1+x)(1+gx)}. \tag{A.4}$$

A.1. Proof of the inequality (7)

For shear rate levels inducing shear-thinning (i.e., for $x > 1$), functions $(1+x)/x$ and $(1+x)^{\beta+1}/x$ are both strictly greater than one. Moreover, the latter attains its minimum value $(1+\beta)^{1+\beta}/\beta^\beta > 1$ at $x = 1/\beta > 1$. As a result, and accounting for relationships (A.2), the following inequality holds

$$0 < S_{\mathrm{BCCY}}(x) = \frac{1-g^\beta}{\frac{1+x}{x}(1-g^\beta)+\frac{(1+x)^{\beta+1}}{x}g^\beta} < \frac{1-g^\beta}{1+g^\beta\left[\frac{(1+\beta)^{\beta+1}}{\beta^\beta}-1\right]} < 1, \tag{A.5}$$

that corresponds to the inequality (7).

A.2. Proof of the inequality (13)

The derivative of Eq. (A.4) with respect to x gives

$$\frac{dS_{\mathrm{SRB}}}{dx} = \frac{(1-t)(1-x^2t)}{(1+x)^2(1+xt)^2}, \tag{A.6}$$

resulting in $\mathrm{sgn}(dS_{\mathrm{SRB}}/dx) = \mathrm{sgn}(1-x^2t)$. Since the function $(1-x^2t)$ is strictly decreasing for $x > 1$ and it vanishes for $x = 1/\sqrt{t}$, the corresponding stationary condition for S_{SRB} corresponds to the maximum value

$$S_{\mathrm{SRB}}\left(\frac{1}{\sqrt{t}}\right) = (1-\sqrt{t})/(1+\sqrt{t}), \tag{A.7}$$

that is the Eq. (14).

In order to prove the inequality (13), let the function $\Delta S(x) = S_{\mathrm{SRB}}(x) - S_{\mathrm{BCCY}}(x)$ be introduced. Since the strict positivity of both the denominators of S_{BCCY} and S_{SRB} when $1 < x < 1/g$, the sign of ΔS coincides with the sign of the following continuous function

$$F(x) = (1-g)[(1-g^\beta)+g^\beta(1+x)^\beta] - (1-g^\beta)(1+gx). \tag{A.8}$$

It can be simply shown that the solutions of the equation $F(x) = 0$ are

$$x_1 = -1, \qquad x_2 = \frac{1}{g}\left(\frac{1-g}{1-g^\beta}\right)^{\frac{1}{1-\beta}} - 1. \tag{A.9}$$

Moreover, due to inequalities in (A.2), the following condition holds

$$\frac{1-g}{1-g^\beta} > \frac{1-g^2}{1-g^\beta} = \frac{1-g}{1-g^\beta}(1+g) > 1+g > (1+g)^{1-\beta}, \tag{A.10}$$

that straight implies $x_2 > 1/g > 1$.

On the other hand, due to the continuity of $F(x)$ and observing that $F(0) = g^\beta - g > 0$, it results

$$\mathrm{sgn}(F) = \mathrm{sgn}(\Delta S) = +1 \qquad \text{for } 1 < x < \frac{1}{g}, \tag{A.11}$$

that is equivalent to the inequality (13).

Data availability

Data will be made available on request.

References

[1] B.M. Johnston, P.R. Johnston, S. Corney, D. Kilpatrick, Non-Newtonian blood flow in human right coronary arteries: steady state simulations, J. Biomech. 37 (5) (2004) 709–720.

[2] P.A. Amorim, M. d'Ávila, R. Anand, P. Moldenaers, P. Van Puyvelde, V. Bloemen, Insights on shear rheology of inks for extrusion-based 3D bioprinting, Bioprinting 22 (2021) e00129.

[3] B. Sauty, G. Santesarti, T. Fleischhammer, P. Lindner, A. Lavrentieva, I. Pepelanova, M. Marino, Enabling technologies for obtaining desired stiffness gradients in GelMA hydrogels constructs, Macromol. Chem. Phys. 223 (2) (2022) 2100326.

[4] R.P. Chhabra, J.F. Richardson, Non-Newtonian Flow and Applied Rheology: Engineering Applications, Butterworth-Heinemann, 2011.

[5] R.B. Bird, R.C. Armstrong, O. Hassager, Dynamics of Polymeric Liquids. Vol. 1: Fluid Mechanics, John Wiley and Sons Inc., New York, NY, 1987.

[6] M.A. Rao, Rheology of Fluid and Semisolid Foods: Principles and Applications, Springer Science & Business Media, 2010.

[7] E.M. Cherry, J.K. Eaton, Shear thinning effects on blood flow in straight and curved tubes, Phys. Fluids 25 (7) (2013).

[8] F.J. Gijsen, F.N. van de Vosse, J. Janssen, The influence of the non-Newtonian properties of blood on the flow in large arteries: steady flow in a carotid bifurcation model, J. Biomech. 32 (6) (1999) 601–608.

[9] R.J. Poole, Inelastic and flow-type parameter models for non-Newtonian fluids, J. Non-Newton. Fluid Mech. 320 (2023) 105106.

[10] A. Waele, Viscometry and Plastometry, Oil and Colour Chemists' Association, 1923.

[11] W. Ostwald, Ueber die geschwindigkeitsfunktion der viskosität disperser systeme. i, Kolloid- Z. 36 (2) (1925) 99–117.

[12] P.J. Carreau, Rheological equations from molecular network theories, Trans. Soc. Rheol. 16 (1) (1972) 99–127.

[13] S. Matsuhisa, R.B. Bird, Analytical and numerical solutions for laminar flow of the non-Newtonian ellis fluid, AIChE J. 11 (4) (1965) 588–595.

[14] M.M. Cross, Rheology of non-Newtonian fluids: a new flow equation for pseudoplastic systems, J. Colloid Sci. 20 (5) (1965) 417–437.

[15] K. Yasuda, Investigation of the analogies between viscometric and linear viscoelastic properties of polystyrene fluids (Ph.D. thesis), Massachusetts Institute of Technology, 1979.

[16] M.T. Gallagher, R.A. Wain, S. Dari, J.P. Whitty, D.J. Smith, Non-identifiability of parameters for a class of shear-thinning rheological models, with implications for haematological fluid dynamics, J. Biomech. 85 (2019) 230–238.

[17] V. Mazzanti, F. Mollica, N. El Kissi, Rheological and mechanical characterization of polypropylene-based wood plastic composites, Polym. Compos. 37 (12) (2016) 3460–3473.

[18] S. Bair, A more complete description of the shear rheology of high-temperature, high-shear journal bearing lubrication, Tribol. Trans. 49 (1) (2006) 39–45.

[19] B.E. Meza, J.M. Peralta, S.E. Zorrilla, Effect of temperature and composition on rheological behaviour and sagging capacity of glaze materials for foods, Food Hydrocolloids 117 (2021) 106689.

[20] K. Godfrey, J. DiStefano III, Identifiability of model parameter, IFAC Proc. Vol. 18 (5) (1985) 89–114.

[21] R. Bellman, K.J. Åström, On structural identifiability, Math. Biosci. 7 (3–4) (1970) 329–339.

[22] J.H. Guillaume, J.D. Jakeman, S. Marsili-Libelli, M. Asher, P. Brunner, B. Croke, M.C. Hill, A.J. Jakeman, K.J. Keesman, S. Razavi, et al., Introductory overview of identifiability analysis: A guide to evaluating whether you have the right type of data for your modeling purpose, Environ. Model. Softw. 119 (2019) 418–432.

[23] A. Raue, C. Kreutz, T. Maiwald, J. Bachmann, M. Schilling, U. Klingmüller, J. Timmer, Structural and practical identifiability analysis of partially observed dynamical models by exploiting the profile likelihood, Bioinformatics 25 (15) (2009) 1923–1929.

[24] G. Santesarti, M. Marino, F. Viola, R. Verzicco, G. Vairo, A quasi-analytical solution for "Carreau-Yasuda-like" shear-thinning fluids flowing in slightly tapered pipes, J. Non-Newton. Fluid Mech. (2025) (submitted) arXiv:2502.14991.

[25] S. Tabakova, N. Kutev, S. Radev, Oscillatory Carreau flows in straight channels, R. Soc. Open Sci. 7 (5) (2020) 191305.

[26] S. Shahsavari, G.H. McKinley, Mobility of power-law and carreau fluids through fibrous media, Phys. Rev. E 92 (6) (2015) 063012.

[27] M. Itskov, et al., Tensor Algebra and Tensor Analysis for Engineers, Springer, 2007.

[28] F. Irgens, Rheology and Non-Newtonian Fluids, vol. 190, Springer, 2014.

[29] Y. Zare, S.P. Park, K.Y. Rhee, Analysis of complex viscosity and shear thinning behavior in poly (lactic acid)/poly (ethylene oxide)/carbon nanotubes biosensor based on Carreau–Yasuda model, Results Phys. 13 (2019) 102245.

[30] M. Ohta, E. Iwasaki, E. Obata, Y. Yoshida, Dynamic processes in a deformed drop rising through shear-thinning fluids, J. Non-Newton. Fluid Mech. 132 (1–3) (2005) 100–107.
[31] Y. Pratumwal, W. Limtrakarn, S. Muengtaweepongsa, P. Phakdeesan, S. Duangburong, P. Eiamaram, K. Intharakham, Whole blood viscosity modeling using power law, Casson, and Carreau Yasuda models integrated with image scanning U-tube viscometer technique, Songklanakarin J. Sci. Technol. 39 (5) (2017).
[32] C. Colosi, S.R. Shin, V. Manoharan, S. Massa, M. Costantini, A. Barbetta, M.R. Dokmeci, M. Dentini, A. Khademhosseini, Microfluidic bioprinting of heterogeneous 3D tissue constructs using low-viscosity bioink, Adv. Mater. 28 (4) (2016) 677–684.
[33] K.A. Aho, Foundational and applied statistics for biologists using R, CRC Press, 2013.
[34] H. Motulsky, A. Christopoulos, Fitting Models to Biological Data Using Linear and Nonlinear Regression: a Practical Guide to Curve Fitting, Oxford University Press, 2004.
[35] P.K. Singh, J.M. Soulages, R.H. Ewoldt, On fitting data for parameter estimates: residual weighting and data representation, Rheol. Acta 58 (2019) 341–359.
[36] A.J. Bailer, C.J. Portier, A note on fitting one-compartment models: Non-linear least squares versus linear least squares using transformed data, J. Appl. Toxicol. 10 (4) (1990) 303–306.
[37] J.B. Freund, R.H. Ewoldt, Quantitative rheological model selection: good fits versus credible models using bayesian inference, Journal of Rheology 59 (3) (2015) 667–701.
[38] J. Cornell, R. Berger, Factors that influence the value of the coefficient of determination in simple linear and nonlinear regression models, Phytopathology 77 (1) (1987) 63–70.
[39] A.C. Cameron, F.A. Windmeijer, An R-squared measure of goodness of fit for some common nonlinear regression models, J. Econometrics 77 (2) (1997) 329–342.
[40] J. Taylor, Introduction to error analysis, the study of uncertainties in physical measurements, 1997.
[41] A.G. Jones, Beyond chi-squared: additional measures of the closeness of a model to data, ASEG Ext. Abstr. 2019 (1) (2019) 1–6.
[42] J. Laborda, S. Ryoo, Feature selection in a credit scoring model, Mathematics 9 (7) (2021) 746.
[43] B.D. Shaw, Uncertainty Analysis of Experimental Data With R, Chapman and Hall/CRC, 2017.
[44] F. Chirianni, G. Vairo, M. Marino, Influence of extruder geometry and bio-ink type in extrusion-based bioprinting via an in silico design tool, Meccanica 59 (8) (2024) 1285–1299.
[45] F. Chirianni, G. Vairo, M. Marino, Development of process design tools for extrusion-based bioprinting: From numerical simulations to nomograms through reduced-order modeling, Comput. Methods Appl. Mech. Engrg. 419 (2024) 116685.
[46] M. Conti, G. Santesarti, F. Scocozza, M. Marino, Models and simulations as enabling technologies for bioprinting process design, in: Bioprinting, Elsevier, 2022, pp. 137–206.
[47] J. Kim, P.K. Singh, J.B. Freund, R.H. Ewoldt, Uncertainty propagation in simulation predictions of generalized Newtonian fluid flows, J. Non-Newton. Fluid Mech. 271 (2019) 104138.
[48] P. Gaziano, M. Marino, Computational modeling of cell motility and clusters formation in enzyme-sensitive hydrogels, Meccanica 59 (8) (2024) 1335–1349.
[49] P. Gaziano, M. Marino, A phase-field model of cell motility in biodegradable hydrogel scaffolds for tissue engineering applications, Comput. Mech. 74 (1) (2024) 45–66.
[50] M. Gierig, P. Gaziano, P. Wriggers, M. Marino, Post-angioplasty remodeling of coronary arteries investigated via a chemo-mechano-biological in silico model, J. Biomech. 166 (2024) 112058.